

# ADVANCES IN THE THEORY OF ATMOSPHERIC FRONTS

I. ORLANSKI, B. ROSS, L. POLINSKY, AND R. SHAGINAW

*Geophysical Fluid Dynamics Laboratory/NOAA*

*Princeton University*

*Princeton, New Jersey*

1. Introduction . . . . .	223
2. Baroclinic Waves and Fronts . . . . .	225
2.1. Quasi-Geostrophic Effects . . . . .	226
2.2. Semigeostrophic Effects . . . . .	228
2.3. Ageostrophic Effects . . . . .	228
3. Mature Front . . . . .	229
3.1. The Significance of Frontal Collapse . . . . .	229
3.2. Dynamic Balance in a Mature Front . . . . .	232
4. What Observed Features Can Be Explained by Theory? . . . . .	233
5. What Other Processes Are Important in Frontogenesis? . . . . .	237
5.1. Structure of the Cold Front . . . . .	237
5.2. Frontogenetical Terms . . . . .	244
References . . . . .	250

## 1. INTRODUCTION

Because so much has been written about atmospheric fronts in extended reviews and textbooks (Pettersen, 1956; Palmen and Newton, 1969; Pedlosky, 1979; Hoskins, 1982), this paper will not attempt to provide a thorough review of the subject, but rather will endeavor to describe breakthroughs in the development of our understanding of fronts\* and to indicate some of the questions yet to be answered satisfactorily. It would be fair to state that the pioneering work of Bjerknes and his collaborators at the Bergen School in the early twenties is to the study of atmospheric fronts what the contemporary work of N. Bohr and his associates in Denmark is to our understanding of atomic structure. The observation by Bjerknes (1919) of convergence lines at boundaries between air masses has had profound implications for theoretical and applied meteorology. Prior to this verification, the possibility that air masses in the atmosphere were separated by surfaces of discontinuity could only be inferred from incomplete observational data. It is quite remarkable, therefore, that Margules (1906) was able to develop a rather detailed theory of atmospheric discontinuities 13 years

\* Although this review will deal with the general subject of atmospheric fronts, primary emphasis will be given to the structure and dynamics of surface cold fronts.

prior to the observational description of Bjerknes. Not only did Margules formulate the theoretical basis for the dynamics of these fronts, but he also recognized the important concept that "the potential energy depends on the horizontal temperature distribution. It appears to be the main source of storm energy and be converted directly into wind [kinetic] energy." But Margules's primary contribution is his well-known formula relating the equilibrium slope  $\alpha$  of the interface between two air masses (1 and 2) having different density  $\rho$  and horizontal wind speed  $U$  along the front:

$$\alpha = (2\Omega/g)[(\rho_2 U_2 - \rho_1 U_1)/(\rho_2 - \rho_1)]$$

where  $\Omega$  is the angular velocity of the rotating frame of reference and  $g$  the gravitational acceleration. This formula was the primary theoretical concept used by the Bergen School to define their observed fronts.

The observations of Bjerknes and his collaborators, using a fairly dense surface network and sparse aerological data, provided the basis for their concept of the evolution of surface cold waves and suggested a link between surface fronts and cyclones. Their results were summarized by Bjerknes (1919) in the classic paper "On the Structure of Moving Cyclones." Eighteen years later, J. Bjerknes (1937) identified the upper-air wave and pointed out its role in cyclogenesis. This discovery led, in turn, to the simultaneous discovery of baroclinic instability by Charney (1947) and Eady (1949). As Charney (1975, p. 11) comments,

At a time when our knowledge of the upper atmosphere was still gained largely by indirect inference from surface observations and from a few upper air ascents, [Bjerknes] accurately described the sequence of events linking the formation of the surface cyclone with the upper wave . . .

Throughout this exciting period of discovery, the more complete picture of the atmosphere provided by new and improved sounding networks offered a continual challenge to the developing theory. In particular, Charney (1975) was puzzled by the fact that whereas a clear correlation had been established between long upper-air waves and primary surface waves, no correspondence had been found between the secondary frontal waves (with wavelength  $\sim 1000$ –2000 km) studied by Bjerknes and Solberg (1921), Solberg (1928), Kotschin (1932), Eliassen (1960), and Orlanski (1968) and the long upper-air waves (with wavelength  $\sim 3000$ –6000 km) described by baroclinic instability theory. Whereas the two-layer numerical experiment of Phillips (1956) demonstrated a link

between baroclinic and surface waves, no similar link has been found between baroclinic waves and waves associated with frontal instabilities.

## 2. BAROCLINIC WAVES AND FRONTS

The primary breakthrough in our understanding of the relationship between surface frontogenesis and the evolution of planetary waves resulted from the primitive-equation numerical simulation described by Phillips (1956). In this numerical solution, growing finite-amplitude baroclinic waves produced regions of more intense temperature gradients suggestive of frontal zones. One could have inferred from this that the deformation field associated with such waves could provide the forcing necessary to produce frontogenesis. The proof of this hypothesis was provided several years later by Williams (1967) in a two-dimensional numerical simulation of the evolution of an Eady wave. Williams showed that the constantly growing, unstable Eady wave produced very intense, frontlike temperature gradients near the surface. After 5 days of model integration, these gradients were so intense as to make the numerical representation, with 50-km horizontal resolution, unacceptably inaccurate.

During the early 1970s, Hoskins and Bretherton (1972) presented an analytic model of frontogenesis that demonstrated how the Eady wave can produce a temperature discontinuity in a finite period of time. In a series of outstanding papers, Hoskins and his collaborators (Hoskins and Heckley, 1981; Hoskins and West, 1979) explained the frontogenetical processes that can occur during the evolution of baroclinic waves. In particular, comparison of the theoretical model results with Williams's numerical solution showed that Hoskins's equation system with the semigeostrophic approximation produced most of the features that Williams's primitive-equation system provided, but with the advantage that an analytic solution could be found for the frontogenesis problem. Furthermore, the Hoskins–Bretherton model generated temperature discontinuities in a finite time without the deficiency of numerical breakdown that Williams encountered.

Hoskins (1982) has reviewed theoretical work on frontogenesis and has summarized recent advances in our understanding of frontogenetical processes in idealized flows. Let us now briefly summarize some of the basic features of frontogenesis using the quasi-geostrophic and semigeostrophic approximations. The processes by which the thermal wind balance along the front is maintained can be better seen from the

equations of the vertical wind shear and horizontal potential temperature gradient, shown here in the  $X-Z$  plane:

$$\begin{array}{cccccc} \text{I} & \text{I} & \text{I} & \text{II} & \text{II} \\ \frac{d_g}{dt}(g\theta_x) = -g\mathbf{V}_{g_x} \cdot \nabla\theta - N^2 W_x - g\mathbf{V}_a \cdot \nabla\theta_x - g\mathbf{V}_{a_x} \cdot \nabla\theta & & & & & (2.1) \end{array}$$

$$\begin{array}{ccccccc} \text{I} & \text{I} & \text{I} & \text{II} & \text{II} & \text{III} \\ \frac{d_g}{dt}(fV_z) = -f\mathbf{V}_{g_z} \cdot \nabla V_g - f^2 U_{a_z} - f\mathbf{V}_a \cdot \nabla V_{g_z} - f\mathbf{V}_{a_z} \cdot \nabla V_g - \frac{d}{dt}(fV_{a_z}) & & & & & & (2.2) \end{array}$$

where

$$\frac{d_g}{dt} \equiv \frac{\partial}{\partial t} + \mathbf{V}_g \cdot \nabla \quad \text{and} \quad \frac{d}{dt} \equiv \frac{\partial}{\partial t} + \mathbf{V} \cdot \nabla$$

The roman numerals above each term indicate the level of approximation assumed. The subscripts  $g$  and  $a$  indicate geostrophic and ageostrophic components, respectively.

Hoskins (1982) uses the quasi-geostrophic (terms I) and semigeostrophic (terms I and II) forms of (2.1) and (2.2) to illustrate how the cross-stream circulation in a very simplified frontal model acts to preserve the thermal wind balance  $fV_{g_z} = g\theta_x$ . In the present discussion, we will show how this balance is maintained for the more realistic jet configuration used by Orlanski and Ross (1977) (Fig. 1) in an integration of the full nongeostrophic equations, starting from idealized geostrophic initial conditions.

### 2.1. Quasi-Geostrophic Effects

The terms  $-g\mathbf{V}_{g_x} \cdot \nabla\theta$  from (2.1) and  $-f\mathbf{V}_{g_z} \cdot \nabla V_g$  from (2.2) each represent the quasi-geostrophic forcing function  $Q_1$  in which the dominant term is  $fU_{g_z}V_{g_x}$ . In the frontal configuration associated with Fig. 1, the along-front wind  $V$  consists of a midtropospheric jet centered above the maximum surface temperature gradient. Therefore  $Q_1$  will be initially antisymmetric about this jet (the shear  $U_{g_z}$  is a positive constant) and positive (negative) to the left (right) of the jet maximum. The cross-stream circulation cells, indicated by dashed lines in Fig. 1, are roughly antisymmetric at the beginning of the integration, a result that is explainable by this symmetry of  $Q_1$  and the use of the quasi-geostrophic approximation (terms I). In this approximation, only the first two terms are retained from the right-hand side of (2.1) and (2.2). If  $Q_1$  is positive (as

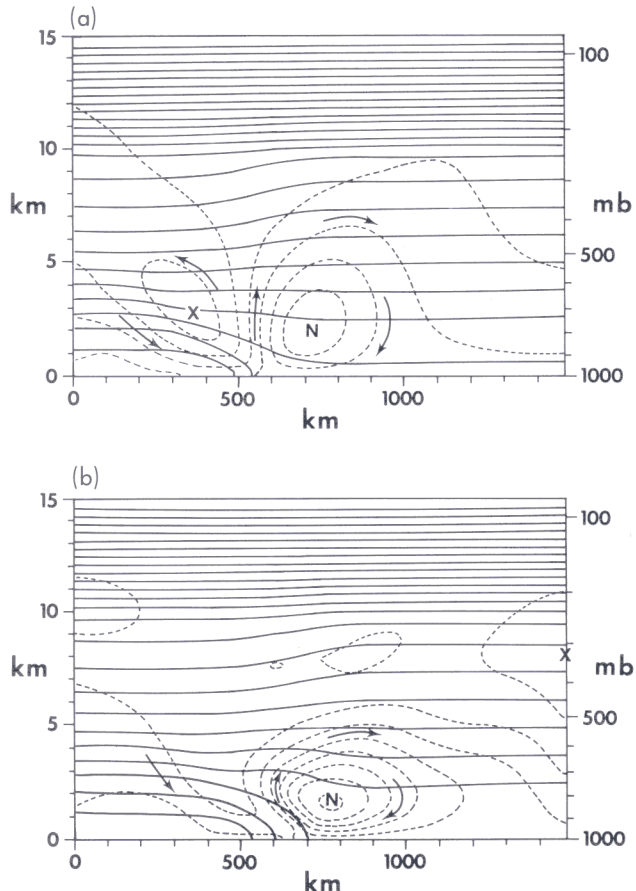


FIG. 1. Plots of potential temperature  $\theta$  (solid contours) and perturbation stream function  $\psi'$  (dashed contours) (a) 3.00 hr and (b) 10.87 hr after a two-dimensional frontal model was initialized with idealized conditions. Locations of maximum and minimum are indicated by X and N, respectively. [After Orlanski and Ross (1977). From *Journal of the Atmospheric Sciences*, copyright 1977 by the American Meteorological Society.]

to the left of the front in Fig. 1), then (2.1) predicts that  $g\theta_x$  will increase (since its forcing term is  $+|Q_1|$ ), while (2.2) indicates that  $fV_{g_z}$  will decrease (since its forcing term is  $-|Q_1|$ ). To counteract this disruption of the thermal wind balance  $g\theta_x = fV_{g_z}$ , an ageostrophic cross-stream circulation develops whereby the third term in (2.1),  $-N^2w_x$ , becomes negative (to the left of the front) to offset the increase of  $Q_1$  in (2.1). Likewise, the third term in (2.2),  $-f^2U_{a_z}$ , becomes more positive to balance  $Q_1$  in (2.2). If cross-front geostrophic balance is assumed to be

maintained, then the quasi-geostrophic terms on the right-hand sides of (2.1) and (2.2) define the diagnostic equation for the cross-stream circulation [as studied by Sawyer (1952, 1956) and Eliassen (1959, 1962)].

## 2.2. Semigeostrophic Effects

As pointed out by Hoskins (1982), the use of the more complete semigeostrophic approximation (terms I and II) produces more realistic asymmetries in the frontal structure. The equation of the vertical component of the relative vorticity  $\zeta$  at the ground  $z = 0$  is

$$\begin{array}{cccc} \text{I} & \text{I} & \text{II} & \text{II} \\ (d_g/dt)\zeta = -fD - \zeta D - \mathbf{V}_a \cdot \mathbf{V}\zeta \end{array} \quad (2.3)$$

For example, under the semigeostrophic assumption, the second term on the right-hand side of (2.3),  $-\zeta D$ , is included in the equation system. As a result, cyclonic vorticity intensifies in convergence zones and weakens in divergence zones, effects that the quasi-geostrophic system cannot produce. Similarly, the semigeostrophic term  $-gU_{ax}\theta_x$  [the last term of (2.1)] enhances temperature gradients in convergence zones and weakens them in divergence zones. Such effects help to produce the asymmetry in frontal features, such as the cross-stream circulation, which is evident in the solution of Orlanski and Ross after 11 hr of integration (Fig. 1b). Figure 1b also shows relative vorticity and horizontal convergence to be maximum at the surface, as one would expect.

The presence of persistent vortex stretching near the surface in the semigeostrophic equations produces an unbounded growth of vorticity until the semigeostrophic approximation is no longer valid (Hoskins, 1982). The semigeostrophic forms of (2.1)–(2.3) do not provide any ageostrophic mechanism by which to prevent this precipitous growth. Certainly the inclusion of eddy diffusion and surface friction can provide a limiting mechanism (Hoskins and Bretherton, 1972).

## 2.3. Ageostrophic Effects

Another possible limiting mechanism, caused by terms neglected in the semigeostrophic approximation, has been proposed by Orlanski and Ross (1984). In the quasi-geostrophic and semigeostrophic approximations, the balance  $f\zeta = \nabla^2 p$  replaces the tendency equation for the horizontal divergence  $D$ . However, if we consider the full equation, then

III      I      I      III

$$(d_g/dt)D = f\zeta - \nabla^2 p - (U_x)^2 \quad (2.4)$$

The approximations discussed in the preceding subsection consider the divergence tendency equation (2.4) to consist of only the first two terms on the right-hand side, namely,  $f\zeta = \nabla^2 p$ . If the rapidly growing vorticity predicted by the semigeostrophic frontogenesis model causes  $f\zeta$  to exceed  $\nabla^2 p$ , then (2.4) with the tendency term included predicts a decrease in convergence ( $D$  becomes more positive), thereby reducing the vortex stretching and helping to limit the unbounded vorticity growth.

In summary, while frontogenetical models are able to explain the rapid frontal intensification, it is still questionable what factors maintain fronts in an approximate steady state for several days, as often is observed in nature.

### 3. MATURE FRONT

Historically, fronts have been viewed as surfaces of discontinuity that separate air masses of different densities. Even in more recent times, the concept of a front as a discontinuity continues to be important, as indicated by the prevalent belief that frontogenetical solutions can only be successful if a discontinuity develops in a finite period of time. In retrospect, Williams's (1967) solution of frontogenesis is seen to have been more successful than was believed at the time of its publication. In 1967 the failure of the frontal solution to produce a discontinuity because of limitations of the finite-difference technique was viewed as a major shortcoming, even though very intense gradients developed in the unstable Eady wave.

#### 3.1. *The Significance of Frontal Collapse*

Why have researchers considered it necessary for fronts to collapse to a discontinuity in a finite time? First of all, it is important that the time scale of the generation of sharp frontal gradients be shorter than the time scale of the baroclinic waves that drive them. In addition, intense gradients imply frontal scales that are much smaller than planetary scales. Accordingly, the time when the solution becomes discontinuous at the surface gives a well-defined, albeit artificial, limit to the frontogenetical solution.

Hoskins and Bretherton (1972), Pedlosky (1979), and Blumen (1981) give a simple argument to explain the development of the discontinuity in the semigeostrophic system. From conservation of potential vorticity and the assumption of semigeostrophy (even for time scales shorter than a pendulum day,  $2\pi/f$ ), it was shown that surfaces of constant  $V$  have constant slopes in the  $x-z$  plane and that these slopes do not vary in time. They therefore conclude that the ageostrophic cross-front wind  $U_a$  should be only a function of the along-front wind  $V$  at the surface; i.e.,  $U_a = F(V)$ . Then the surface convergence  $U_{ax}$  should be proportional to vorticity  $V_x$  since  $U_{ax} = F_V(V)V_x$ . In this case the term  $-\zeta D$  in the vorticity equation (2.3) will be the positive quantity  $-\zeta^2 F_V$  assuming  $F_V < 0$ ; therefore vorticity growth will be unbounded.

Theoretical studies of other nonlinear systems (Witham, 1974; Boyd, 1980) have demonstrated that nondispersive waves can develop discontinuities in finite times. What factors determine the conditions under which geophysical fluids will develop similar discontinuities? In its simplest form, the shallow-water equation system can be shown to produce wave breaking due to differential advection of the wave crest and trough (Boyd, 1980). A simplified set of equations, relevant to the surface front, can be obtained from the inviscid momentum equations on a flat surface (so that  $w = 0$ ):

$$(d/dt)U_a - fV_a = 0 \quad (3.1)$$

and

$$(dV/dt) + fU_a = 0 \quad (3.2)$$

Solutions to (3.1) and (3.2) can be determined for two different limits. First, if we assume  $V_a \equiv 0$  (i.e.,  $\nabla \equiv V_g$ ), then (3.1) reduces to

$$(dU_a/dt) = (\partial U_a/\partial t) + U_a(\partial U_a/\partial x) = 0$$

This is the equation studied by numerous authors, e.g., Witham (1974); it produces a discontinuity in a finite time. In the other extreme, we may assume that  $V = V_a$  so that  $V$  is completely nongeostrophic. A complete steady-state solution can then be found to this nonlinear system, namely,

$$[U_0^2 - U^2(x, t)]^{1/2} + C \arcsin \frac{U(x, t)}{U_0} = \pm(x - ct)f \quad (3.3a)$$

$$V = \mp[U_0^2 - U^2(x, t)]^{1/2} \quad (3.3b)$$

where

$$|U(x, t)| < |U_0|$$

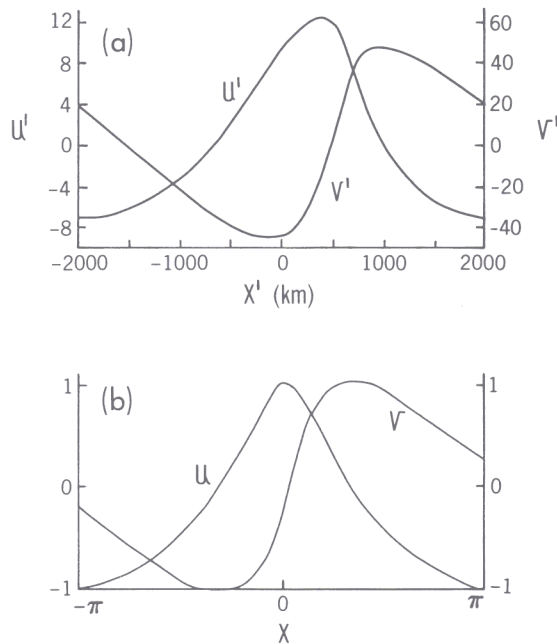


FIG. 2. (a) Distribution of across-front velocity  $U'$  and along-front velocity  $V'$  at a height of 0.5 km after 5 days of integration of a primitive equation, 2-D frontal solution. [After Williams (1967). From *Journal of the Atmospheric Sciences*, copyright 1967 by the American Meteorological Society.] (b) Distribution of quantities  $U$  and  $V$  from equation (3.3) described in the text. Primed quantities are dimensional, while unprimed variables are nondimensional.

The tendency  $\partial/\partial t$  has been replaced by  $C(\partial/\partial x)$ , with  $C$  a constant propagation speed.\* Equation (3.3) (plotted in Fig. 2b) shows a remarkable similarity to the fields at  $z = 500$  m (Fig. 2a) from Williams's (1967) solution. Since this solution represents a nonlinear steady-state result like a hydrodynamic bore propagating with constant phase speed  $C$  and does not exhibit collapsing characteristics, one would expect that Williams's frontal solution would have gone to this steady solution, rather than to the limit of frontal collapse, if numerical inaccuracies were not present.

Some solutions by Houghton (1969) of the shallow-water equations with rotation are also very relevant to this discussion. These equations were found to exhibit a collapsing character if inertial waves are suppressed; i.e.,  $f = 0$ . Inclusion of the dispersive ageostrophic effects

\* If  $C \gg U_0$ , the solution reduces to a linear inertial wave.

when rotation is present leads to a more balanced solution such as (3.3). One may then conclude from the preceding simple models that the occurrence of discontinuities in a finite time is largely the result of approximations applied to the primitive equations. These approximations apparently can eliminate dispersive effects such as inertial waves that tend to prevent frontal collapse.

### 3.2. Dynamic Balance in a Mature Front

The possible frontolytical effect of ageostrophic processes is an important element in our understanding of the dynamics of mature, quasi-steady fronts. Such ageostrophic mechanisms provide an alternative to the widely held view that discontinuities can only be prevented through the inclusion of diffusive effects (Williams, 1974). As explained in Section 2, the full divergence tendency equation (2.4) shows that as vorticity increases due to vortex stretching in areas of low-level convergence, negative feedback produces divergence tendency, thereby reducing convergence and vortex stretching. This effect thus produces a phase shift between the vorticity and divergence maxima and reduces the need for viscous dissipation to damp vorticity growth (Orlanski and Ross, 1984).

When considering the dynamic balances in a mature front, it is important to consider not only the dynamic response of the front to an imposed large-scale deformation field, but also the intensity of the synoptic-scale forcing itself. For example, although the two-dimensional front models treated numerically by Williams (1967) and Orlanski and Ross (1977) appear to have many similar features, Williams's solution experiences continuous frontogenetical growth, whereas the front in Orlanski and Ross's model evolves into a mature, quasi-steady state (Fig. 1b) after an initial period of frontogenetical adjustment. These dramatic differences are explainable by differences in the configurations used to initialize each model. The Eady wave used in Williams's initial conditions is unstable, even in its finite-amplitude state. The stability criterion for this Eady wave is dependent on the horizontal wavelength in that Eady waves are neutrally stable when their wavelength is less than roughly 2000 km, as is the case in the solution of Orlanski and Ross (1977). Accordingly, Williams's synoptic-scale disturbance is constantly intensifying, so one would expect the front embedded in this field to exhibit a similar growth. On the other hand, the fact that the Orlanski–Ross front remains effectively steady in a neutral wave demonstrates that finite-amplitude, slowly growing baroclinic waves can support frontal regions in a quasi-

steady configuration. Many of the long-lived fronts observed in the real atmosphere may fall into this category.

Standing issues that still remain to be resolved regarding mature fronts are (1) what dynamic balance between frontogenetical and frontolytical processes occurs in realistic long-lived fronts, and (2) what determines the characteristic scale of such fronts? We will attempt to answer the first later in this chapter.

Regarding the latter question, it is well known that the aspect ratio between the depth and width of a surface front is of order  $N/f$ , where  $N$  is the Brunt–Väisälä frequency. Stated in a slightly different way, the frontal width is the order of the Rossby radius of deformation, while the height is determined by the depth of penetration of the front (Orlanski and Polinsky, 1983).

Figure 3 shows a comparison among the analyzed vertical structures of three different observed fronts. The moderately intense cold front analyzed by Ogura and Portis (1982) (Fig. 3a) has a horizontal scale near the surface on the order of 200 km. Sanders's (1955) front (Fig. 3b) is considerably more intense, with horizontal scales of 50 km or less. Finally, the time–height cross section of potential temperature shown in Fig. 3c is taken from microwave radiometer measurements described by Decker (1984) during the passage of a cold front aligned perpendicular to, and east of, the Rocky Mountains. The frontlike structure shown exhibits two horizontal scales, the wider one passing in a time of order 50 min and the narrower one in about 4 min.

The fronts shown in Figs. 3a and 3b are more classic in their structure and horizontal scales, while the “front” in Fig. 3c is similar to the “Southerly Buster” described by Baines (1980) as a Kelvin jet flow that forms ahead of cold fronts in the presence of orography. These three fronts show the wide range of scales exhibited by fronts observed in nature.

#### 4. WHAT OBSERVED FEATURES CAN BE EXPLAINED BY THEORY?

The extensive observational studies of the Bergen School that confirmed the existence of surface fronts did not, of course, reveal the structure of the cross-stream circulation associated with frontal surfaces. In fact, this circulation was inferred from quasi-geostrophic theoretical considerations by Sawyer (1952, 1956) and Eliassen (1959, 1962) rather than from the sparse upper-air data existing at that time. This theory indicates that whenever the horizontal temperature gradient increases in

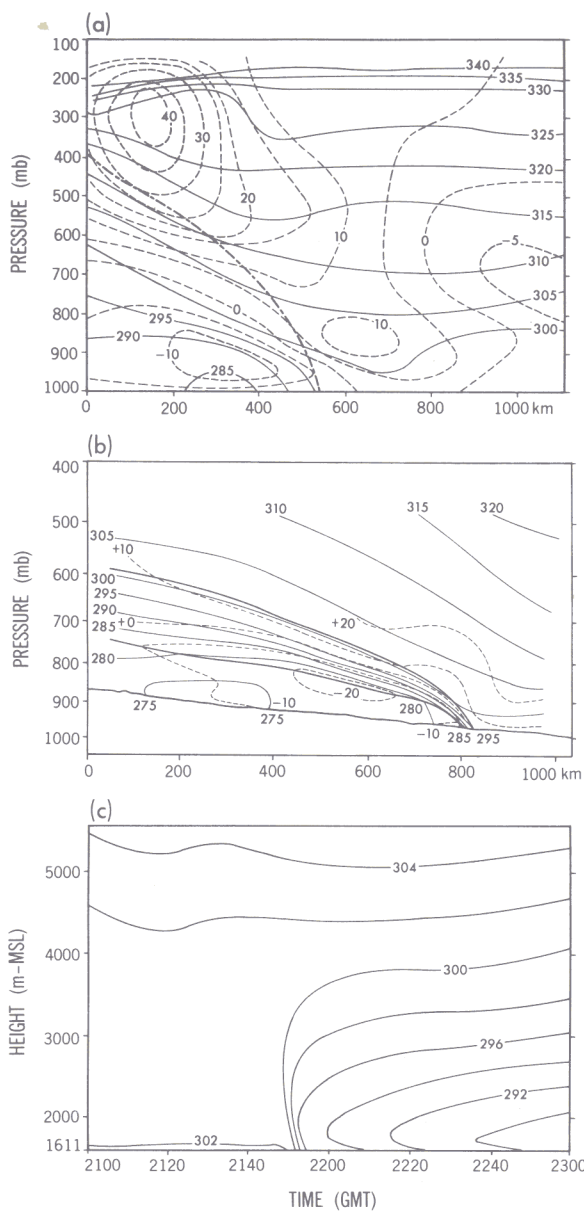


FIG. 3. (a) Vertical cross section of potential temperature (solid contours) and along-front velocity (dashed contours) for observed cold front. Heavy dash-dot line indicates line of maximum vorticity. [After Ogura and Portis (1982). From *Journal of the Atmospheric Sciences*, copyright 1982 by the American Meteorological Society.] (b) Cross section of potential temperature (solid contours) and along-front velocity (dashed contours) for observed front. Heavy solid lines indicate boundaries of frontal zone. [After Sanders (1955). From *Journal of Meteorology*, copyright 1955 by the American Meteorological Society.] (c) Time-height cross section of potential temperature as observed by microwave radiometer measurements. [After Decker (1984).]

the front as a result of differential advection in a horizontal deformation field, a thermodynamically direct vertical circulation must develop in order to produce a corresponding increase in the vertical wind shear. It is through this vertical circulation that the mesoscale and synoptic-scale features of the frontal system interact.

The horizontal scale of the frontal waves discussed in Section 1 is an order of magnitude larger than the mesoscale features of the cross-stream frontal circulation. It is only recently that the use of dense observing networks has enabled scientists to determine simultaneously the three-dimensional structure of the wind and temperature fields and thereby to obtain more evidence of the processes that act to produce, maintain, and ultimately destroy the sharp temperature gradients within frontal surfaces. Nevertheless, since the atmospheric front is one of the most prevalent features of extratropical weather maps, it is surprising that only a few attempts have been made to examine in detail these frontogenetical and frontolytical processes in actual observed fronts. An early effort to do this was made by Sanders (1955) in a case study of an intense surface cold front. His careful analysis of data from a rather dense observing network indicated that air that enters the front from the warm air zone near the surface experiences frontogenetical intensification one to two orders of magnitude larger than typical in the free atmosphere. As this air moves up the isentropes within the frontal zone, frontolytical effects act to weaken temperature and wind gradients, thereby producing the typical frontal structure in which gradients are maximum close to the surface.

Because of the apparently realistic behavior of the Hoskins-Bretherton (referred to here as HB) frontogenesis model, Blumen (1980) has made a one-to-one comparison of the predictions of this idealized model and Sanders's analysis. He found qualitative agreement regarding details of the horizontal wind and temperature fields. Major discrepancies were evident, however, in the details of the vertical frontal circulation itself. In particular, the vertical velocity, which was most intense at the middle levels of the model, was less intense and broader in scale than the narrow rising jet that Sanders's analysis showed to occur above the zone of maximum cyclonic vorticity within the surface front. As Blumen has pointed out, this narrow jet produces the most significant frontogenetical effects in the observed front by vertically tilting isentropic surfaces and isopleths of the horizontal long-front wind. An explanation of the discrepancies between model and observations was demonstrated by Blumen to be due to the absence of a boundary layer and turbulent mixing processes within the model.

More recently, observations from the dense upper-air network of the 1979 SESAME/AVE field experiment have permitted Ogura and Portis

(1982) to produce a more coherent picture of observed mesoscale features of a cold front. This study analyzes a cold front that passed through the SESAME network on 25–26 April 1979. Although severe storms formed along the surface front during this period, the Ogura–Portis analysis of frontogenetical and frontolytical effects in the cross-stream circulation is limited to adiabatic processes.

This analysis indicates a direct cross-stream vertical circulation, with moist air ascending above the surface front but with the upgliding flow within the frontal zone encountering a secondary circulation at midlevels. Also the horizontal temperature gradient and vertical vorticity are maximum near the ground, as predicted by the HB model and observed by Sanders (1955). The fact that the horizontal temperature gradient is smaller in the warm, rather than the cold, sector is also stressed as agreeing with the HB model prediction as calculated by Blumen (1980).

The theoretical model fails to predict other important observed features. Specifically, the observed horizontal convergence and cyclonic vorticity are the same order of magnitude and are concentrated in zones of similar widths (approximately 300 km). Also, as pointed out by Blumen's comparison with Sanders's analysis, the vertical ascending motion analyzed by Ogura and Portis is located at low levels within the front, rather than the middle levels as the HB model predicted. A close comparison of the adiabatic frontogenetical functions was done only with Sanders's results. Both sets of results are qualitatively similar although the magnitudes of Sanders's terms are an order of magnitude larger because of his more intense front. Only the general structure of the vertical circulation was compared with the HB results.

In summary, both Blumen's analysis of Sanders's results and Ogura and Portis's analysis show qualitative agreement in coarser observed frontal features with the HB model results but fail to show agreement in important details such as the structure of the vertical motion field and the effect of frontogenetical and frontolytical forcing. Even the inclusion of Ekman pumping in the planetary boundary layer (Blumen, 1980) was unable to produce a realistic vertical jet as is observed. Such disagreement is not surprising in view of the simplifying assumptions of semigeostrophy and two-dimensionality in the model and the absence of realistic processes such as moist convection and turbulent mixing. The important question to be addressed is which of these missing elements is needed to make the theoretical simulation of the cold front more realistic? This question points out the serious gap that remains in our understanding of the processes that govern frontal dynamics.

## 5. WHAT OTHER PROCESSES ARE IMPORTANT IN FRONTOGENESIS?

In attempting to include all of the processes that are important in frontogenesis, one realizes that it is no longer possible to employ a simple idealized frontal model. Some of these processes that are regarded as important are the effect of moisture on the frontal environment, the interaction of convective systems with the frontal circulation, and the influence of the planetary boundary layer. These phenomena are notoriously difficult to include as simple parameterizations (Rao, 1966; Orlanski and Ross, 1977; Ross and Orlanski, 1978; Blumen, 1980; Keyser and Anthes, 1982). In addition, the most widely used assumption of all, the approximation of two-dimensionality, may also be questioned.

Today, with the availability of high-speed computers, we now have the capability to produce model simulations of observed fronts with most of these important processes included. Recent simulations of the evolution of a cold front in a moist environment (Ross and Orlanski, 1982; Orlanski and Ross, 1984) have produced realistic mesoscale features such as the presence of dual updrafts similar to those analyzed in observed squall lines. Unfortunately, in the case study described by Ross and Orlanski, observations could not be analyzed in sufficient detail to warrant an intercomparison with the cross-stream circulation in the model solution. In fact, the literature contains very few detailed comparisons of mesoscale model results with observations.

Recent observational experiments using dense observing networks [e.g., Severe Environment Storm and Mesoscale Experiment (SESAME)] now can provide a more complete picture of the mesoscale structure of fronts. The existence of these observational data sets and the availability of three-dimensional mesoscale numerical models offers us the opportunity for a detailed comparison of modeled fronts (including frontogenetical processes) with their observed counterparts. Therefore, we will present in this section a comparison of a new mesoscale numerical simulation with the analysis by Ogura and Portis (1982) of the SESAME cold front of 25–26 April 1979.\*

### 5.1. Structure of the Cold Front

The formulation of the model used here has been described in detail by Ross and Orlanski (1982). The specific form of the model, including recent

\* Anthes *et al.* (1982) have also provided a numerical simulation of this case; however, they did not attempt to compare their results with Ogura and Portis's results.

modifications, is described by Orlanski and Polinsky (1984). The model is initialized at 0000 GMT 25 April 1979 from the GFDL/FGGE (First GARP Global Experiment) global analysis over a domain covering the eastern two-thirds of the United States. Boundary data, only used locally where inflow occurs, are obtained by the same initialization procedure, using the GFDL/FGGE analysis at synoptic times (0000 GMT and 1200 GMT).

Due to space limitations, we will confine our discussion to those features of the observed front described by Ogura and Portis (1982).<sup>\*</sup> Our primary intent is to make a detailed one-to-one comparison of model results with their analysis.

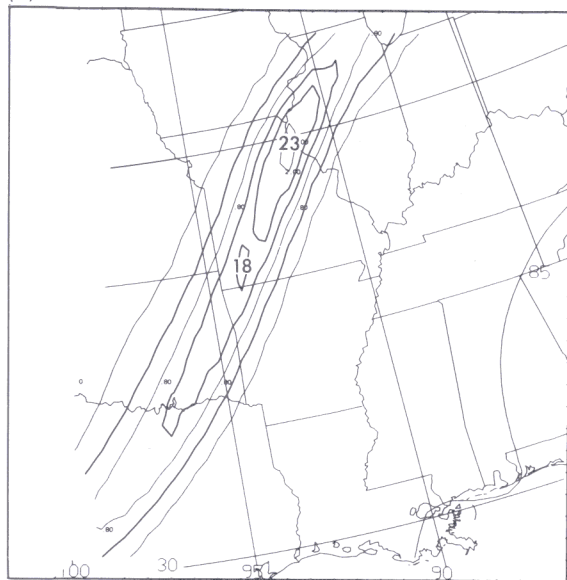
The broad features of the observed front, such as frontal position, geopotential height, and wind field structure, are well simulated by the model. In fact, a close comparison of the mesoscale solution with either the GFDL/FGGE or the National Meteorological Center (NMC) operational analysis would not be appropriate due to the great disparity between model and observing network resolutions. On the other hand, the OP analysis of the dense SESAME network observations provides a more useful test of the validity of the current mesoscale simulation.

As in OP, we will confine our discussion to the time 0200 GMT 26 April 1979, which is 26 hr into the model integration. Apparently, this time was chosen by Ogura and Portis because it corresponded to the beginning of severe convection along the cold front. The vertical component of the surface relative vorticity in the simulation [Fig. 4a (OP8)] shows the same frontal alignment as that observed. A cellular structure appearing on the analyzed vorticity field is far less pronounced in the simulation. General agreement is found between strong temperature gradients, vorticity [Fig. 4a (OP8)], and surface convergence [Fig. 4b (OP9)]. An important finding of OP was that the analyzed surface maxima of convergence and vorticity were of roughly the same magnitude. This was a major discrepancy between OP's analysis and idealized theoretical models, which predicted much weaker convergence compared to vorticity. Although the present model simulation shows good agreement with OP in the magnitude of the convergence, the simulated vorticity maximum is twice as large.

The absence of precise mesoscale observations regarding the position of the front and its associated convection requires that some aspects of the model results be compared with detailed satellite photographs. To a first approximation, the location and column-integrated content of liquid water in the model solution can be related to corresponding satellite imagery. Figure 5 (OP20) provides such a comparison. Allowing for

\* This paper will also be referred to here as OP. Their figures will be designated by OP followed by their figure number.

(a)



(b) A

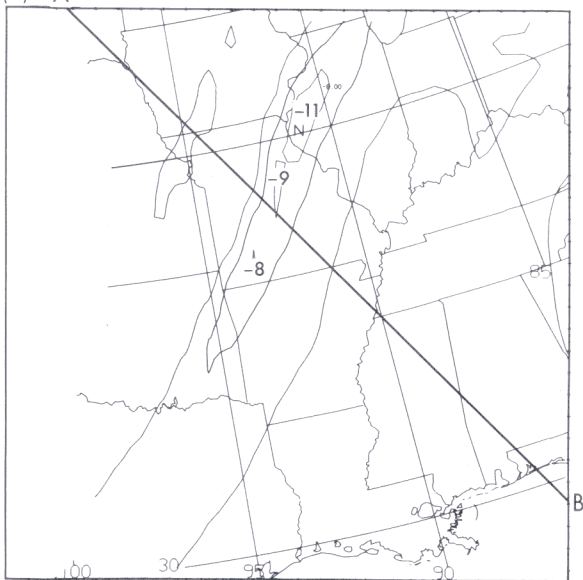


FIG. 4. (a) Horizontal distribution of vertical vorticity (units of  $10^{-5} \text{ s}^{-1}$ ) at height  $z = 0$  m from frontal simulation at 0200 GMT 26 April. Region where surface is above 500 m height is not contoured. (b) Distribution of horizontal divergence (units of  $10^{-5} \text{ s}$ ) at height  $z = 0$  m. Line segment A–B indicates cross section used in later figures.

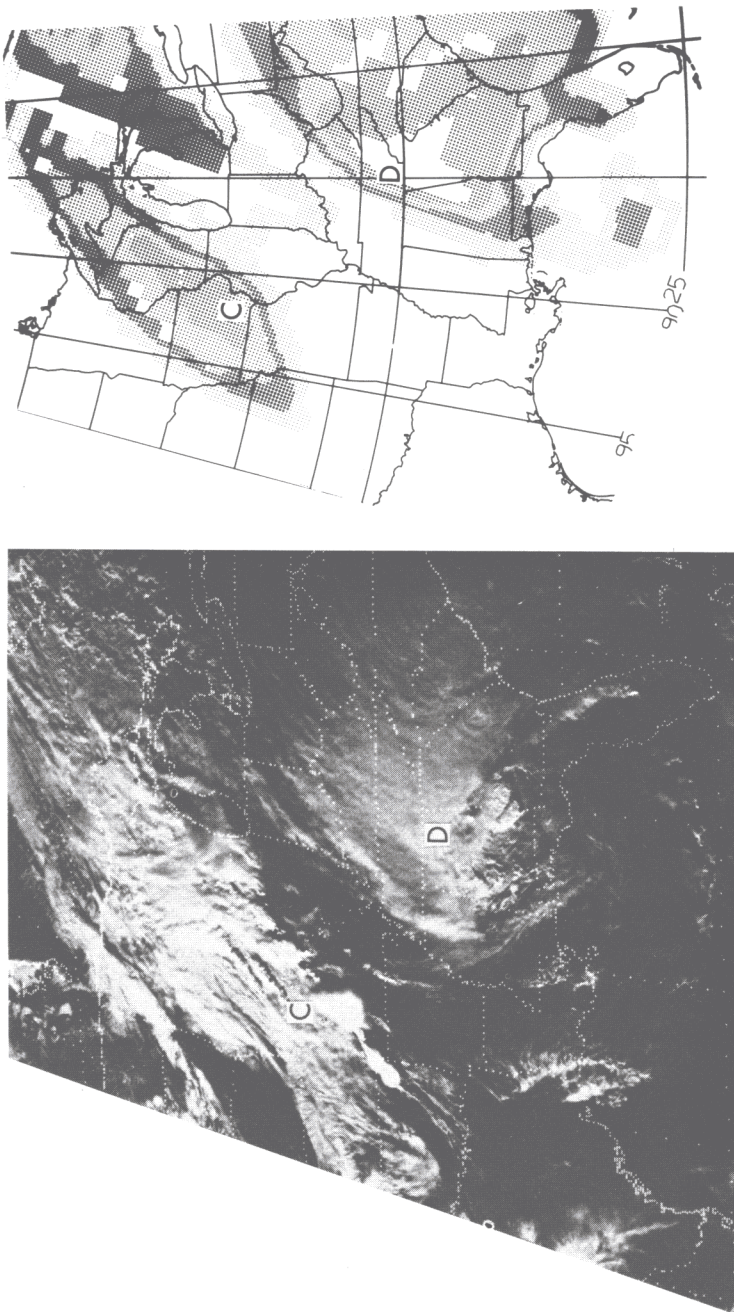


FIG. 5. Comparison of satellite photograph of 2301 GMT 25 April with cloud distribution from model simulation. Letters C and D indicate corresponding weather systems in each frame. (Photograph courtesy of Y. Ogura.)

differences in mapping between satellite and model results, one can see good agreement in position for the two major cloud zones, labeled C and D. Cloud system C is associated with the frontal system under discussion here. Locations of intense precipitation zones (not shown here or in OP) show good agreement for the two storm systems C and D.

The structure of the frontal circulation is shown in Fig. 6 (OP17, OP21) in a vertical cross section perpendicular to the frontal system along the line AB of Fig. 4b. The position of this line is similar to but several hundred kilometers north of that chosen by OP. Striking similarities and some differences are evident between this structure and OP's results. The upper-level jet maximum, analyzed by OP to be  $40 \text{ m s}^{-1}$ , is only  $30 \text{ m s}^{-1}$

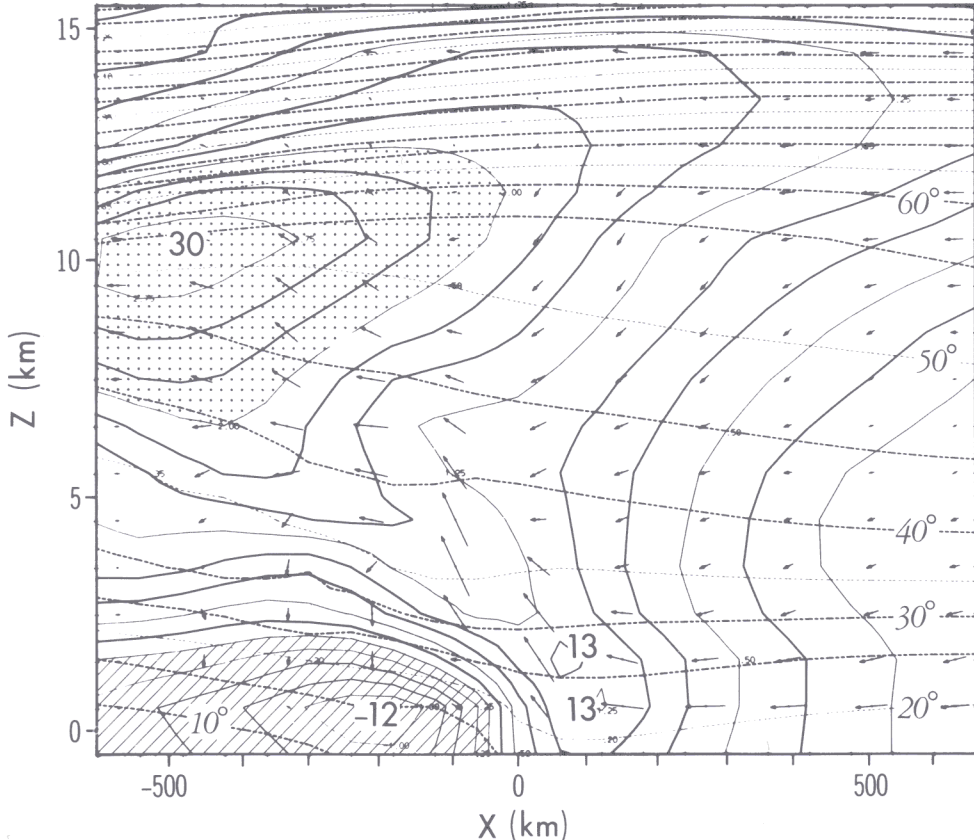


FIG. 6. Vertical cross section (line A–B of Fig. 4b) of along-front velocity  $V$  (solid contours) and potential temperature (dashed contours) from simulation at 0200 GMT 26 April. Vectors denote cross-front velocities. Stippled region indicates  $V > 20 \text{ m s}^{-1}$ . Cross-hatching indicates  $V < 0 \text{ m s}^{-1}$ .

here. (The GFDL/FGGE analysis shows only  $27 \text{ m s}^{-1}$ .) Nevertheless, the region in which winds exceed  $20 \text{ m s}^{-1}$  (stippled zone in Fig. 6) is similar in extent to that of OP.

The similarities between the two fields for the lowest 5 km are remarkable. Predominant features are a northerly surface jet (at 950 mb or 500 m) to the left of the strong temperature gradients and a southerly low-level jet ahead of the front (at 850 mb or 1500 m). The southerly jet ahead of the front has been frequently observed and was speculated by Keyser and Anthes (1982) to be the result of planetary boundary layer effects. We would suggest, however, that the presence of moist convection could also play an important role, since a similar solution produced without moisture for the present case did not show this low-level jet.

The circulation within the plane of the cross section, indicated in Fig. 6 by vectors, includes the removal of a  $10\text{-m-s}^{-1}$  rightward translation, corresponding to the assumed translation of the cold front (as in OP21). Similarities with observations are apparent, including inflow of warm air into the front at low levels, upgliding motion on an incline steeper than the isentropes, and sinking motion in the cold air to the rear of the front. A primary difference is the simulated weak downward motion ahead of the upper-level jet, which does not appear in the OP analysis. This sinking motion appears to be associated with the low-pressure system to the southeast of this domain (cloud system D in Fig. 5). Conceivably, the OP analysis of vertical motion was unable to capture this feature.

Distinguishing features of the frontal zone as a separate entity from the larger baroclinic system are clearly evident in the vorticity, the vertical velocity, and the magnitude of the potential temperature gradient as shown in the vertical cross sections in Fig. 7. The vertical component of vorticity [Fig. 7a (OP18)] has a similar structure to observations. Two maxima of cyclonic vorticity are identifiable, one due to the upper-level jet and the other associated with the surface front. The magnitude of the calculated frontal vorticity is double its analyzed value, as mentioned in the discussion of Fig. 4a. Although such differences might be considered to be acceptable, we believe that such disparities may reflect the coarseness of the observing network used by OP.

The vertical velocity field [Fig. 7b (OP19)] shows dual updraft maxima similar to the observed maxima in OP's figure at 650 and 950 mb. Although direct quantitative comparison between simulated and observed fields of upward motion is difficult because of differences in analyzed quantities (velocity  $w$  in  $z$  coordinate versus velocity  $\omega$  in  $p$  coordinate), a rough comparison indicates the model upward motion to be twice as intense as its analyzed equivalent. The sinking motion to the rear of the

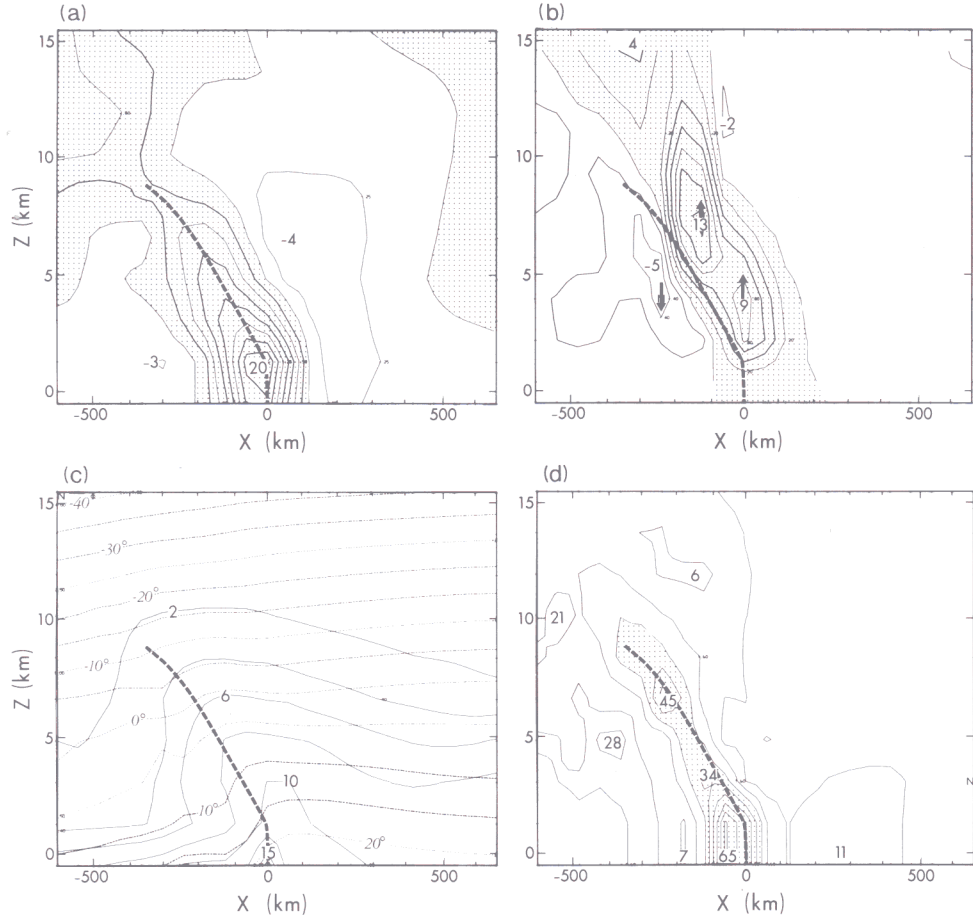


FIG. 7. Comparison of fields in cross section A–B (Fig. 4b) for (a) vertical vorticity ( $10^{-5} \text{ s}^{-1}$ ), (b) vertical velocity ( $10^{-2} \text{ m s}^{-1}$ ), (c) water vapor (solid contours,  $\text{gm kg}^{-1}$ ) and temperature (dashed contours,  $^{\circ}\text{C}$ ), and (d) horizontal potential temperature gradient  $|\nabla_H\theta|$  ( $10^{-6} \text{ K m}^{-1}$ ). Stippled areas indicate positive fields in (a) and (b) and values greater than  $24 \times 10^{-6} \text{ K m}^{-1}$  in (d). Heavy dashed line indicates lines of maximum vorticity.

front agrees with observations. Ahead of the front, the simulation shows sinking motion of less than  $2 \text{ cm s}^{-1}$ , whereas the analysis shows slightly larger intensity and more variability.

Note that the position of the frontal zone, defined as the line of maximum cyclonic vorticity and indicated in Fig. 7 by a heavy dashed line, shows a vertical penetration (to 5 km) similar to that determined from observations (see OP18 and neglect that portion of the vorticity

maximum line that is associated with the upper-level jet). The position of the strong upward motion occurs to the right of this vorticity line (Fig. 7b). Finally, the cross section of water vapor mixing ratio and temperature [Fig. 7c (OP16)] shows reasonable agreement with observations.

The region of largest horizontal potential temperature gradient  $|\nabla_H\theta|$ , shown by stippling in Fig. 7d, overlaps the line of maximum vorticity. A point we will stress below in comparing dry and moist solutions is that the slope of the vorticity line as well as the region of large  $|\nabla_H\theta|$  are much steeper than the potential temperature contours, as seen in Fig. 7d. This can also be seen in the vectors above the surface front in Fig. 6. An analysis of this solution indicates that fluid parcels in the moist environment will tend to follow lines of constant equivalent potential temperature in the same manner as they follow constant- $\theta$  lines in the dry case. This conclusion that the moist environment can directly change the circulation of the front is an important result.

### 5.2. Frontogenetical Terms

To this point in the discussion, emphasis has been given to the extent to which the 26-hr simulation results agree with the detailed observational analysis of OP. However, one of the goals of this study will be to utilize the completeness of this numerical solution to provide insight into the role of the various frontogenetical and frontolytical forcing mechanisms in the maintenance of the front. To this end, the analysis of those terms that enhance or weaken potential temperature gradients may provide us with clues as to which processes are most important. Following Miller (1948), Sanders (1955), and others, one may derive a prognostic equation that describes the time variation of the magnitude of the horizontal gradient of potential temperature  $|\nabla_H\theta|$ . A frontogenetical function may then be defined as  $(d/dt)|\nabla_H\theta|$ , the time rate of change of  $|\nabla_H\theta|$  following a fluid parcel. This is similar to the leftmost term of (2.1). The basic equation for the conservation of potential temperature may be differentiated in the horizontal to obtain an expression for this frontogenetical function:

$$\frac{d}{dt} |\nabla_H\theta| = \text{CONVERGENCE} + \text{DEFORMATION} + \text{TILTING} + \text{DIFFUSION} + \text{DIABATIC} \quad (5.1)$$

where

$$\text{CONVERGENCE} \equiv -\frac{1}{2|\nabla_H\theta|}(\theta_x^2 + \theta_y^2)(U_x + V_y)$$

$$\text{DEFORMATION} \equiv -\frac{1}{2|\nabla_H \theta|} [(\theta_x^2 - \theta_y^2)(U_x - v_y) + \theta_x \theta_y (U_y + V_x)]$$

$$\text{TILTING} \equiv -\frac{\theta_z}{|\nabla_H \theta|} [\theta_x w_x + \theta_y w_y]$$

$$\text{DIFFUSION} \equiv \frac{1}{|\nabla_H \theta|} [\nabla_H \cdot \nabla F]$$

and

$$\text{DIABATIC} \equiv \frac{1}{|\nabla_H \theta|} [\nabla_H \theta \cdot \nabla H]$$

The quantity  $F$  is the diffusion term in the original prognostic equation for  $\Theta$ , and  $H$  is the heating due to condensation/evaporation.

Both Sanders (1955) and OP have attempted to evaluate the first three (adiabatic) terms on the right-hand side of (5.1) for observed fronts. Also, Blumen (1980) has evaluated these adiabatic terms for the idealized Hoskins–Bretherton model of a dry front. We feel that it is important to clarify the role of the other terms, namely, the diabatic and the diffusive terms, in the context of our observed front simulation.\* To make the effects of moisture more apparent, we will also compare terms in the complete moist solution with those from a solution in which moisture is excluded.

Figure 8 shows a comparison between the dry and moist solutions of the convergence, deformation, and tilting terms,† which are the only contributors to the frontogenetical function in the term-by-term analyses of the three papers mentioned earlier. The moist terms in Fig. 8 should be compared to those shown by OP (OP25) for the same time. In order to provide an uncluttered view of the structure in both the moist and dry cases, we use different contour intervals (as indicated in the upper-right-hand corner of each frame) in each case.

An inspection of Fig. 8 reveals that corresponding terms for the dry and moist cases have the same signs at low levels in each case. Specifically, convergence and deformation are both frontogenetical, while tilting is frontolytical near the surface. At these levels, the magnitudes of the moist terms are three to four times larger than the corresponding dry terms. The similarity between terms ends above 1.5 km in conjunction with the

\* All terms shown here were averaged over 30 min (15 time steps) of model integration.

† Palmen and Newton (1969, p. 261) have also noted the potential importance of diabatic effects that could not be analyzed in Sanders's (1955) study. (The authors thank Dan Keyser for pointing out this reference to them.)

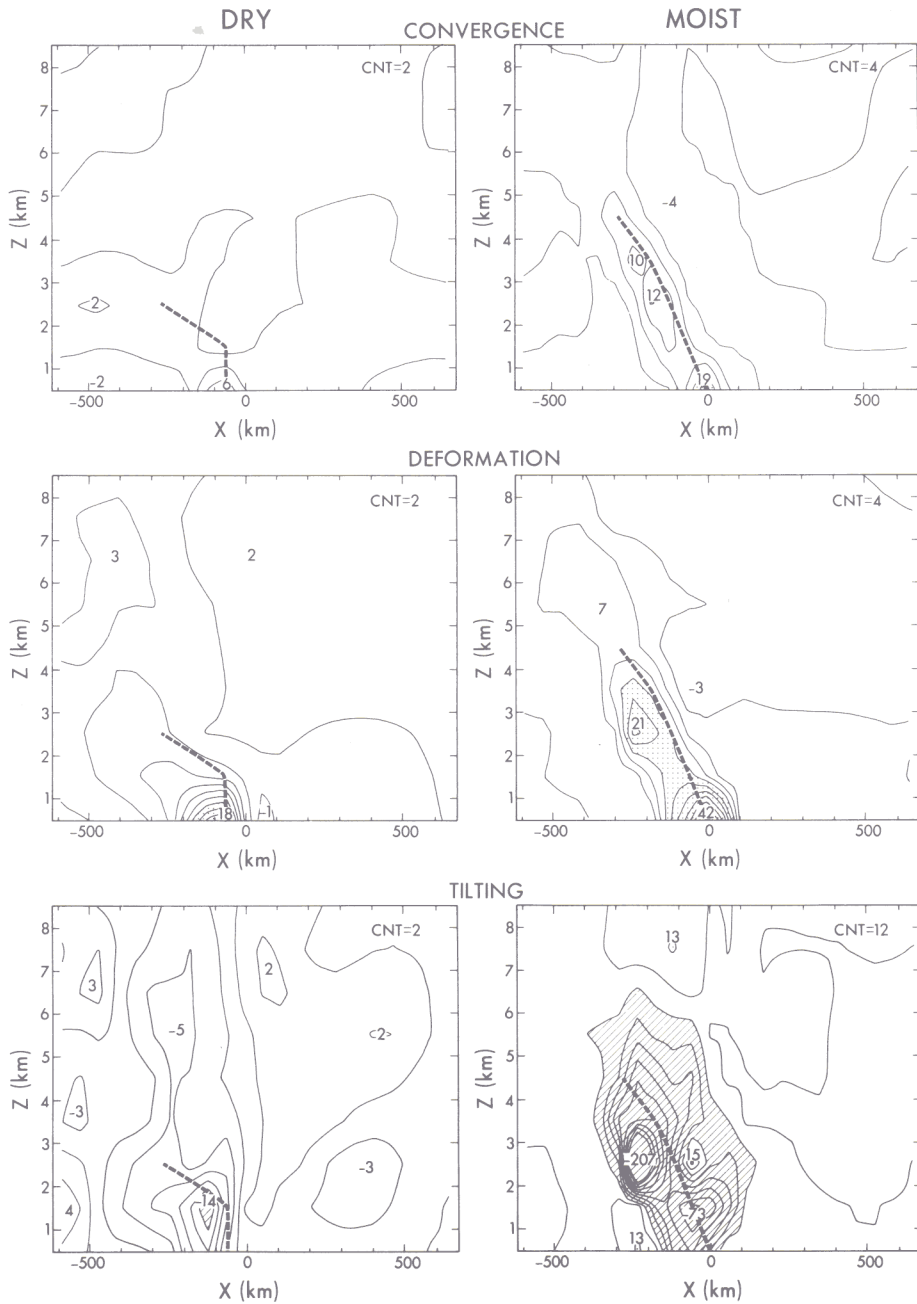


FIG. 8. Comparison of adiabatic terms from dry and moist simulations at 0200 GMT in vertical cross section A-B (Fig. 4b). Contour interval for each frame is shown in upper right corner in units of  $10^{-10} \text{ K m}^{-1} \text{ s}^{-1}$ . Cross-hatching and stippling indicate terms less than  $-12 \times 10^{-10} \text{ K m}^{-1} \text{ s}^{-1}$  and more than  $12 \times 10^{-10} \text{ K m}^{-1} \text{ s}^{-1}$ , respectively.

separation of the dry and moist vorticity maximum lines (dashed lines, defined as in Fig. 7). In fact, the shallower slope of the vorticity lines in the dry, compared to moist, solutions is another indication of the tendency of the fluid parcels to follow isentropes in the dry case and isolines of equivalent potential temperature in the moist case. Certainly, deeper penetration of the front is a dominant feature of the moist solution.

Comparison of the moist terms in Fig. 8 with those of OP (OP25) show very good agreement with regard to sign, vertical penetration, and general structure. The increased intensity of the simulated terms in comparison with the analyzed terms is consistent with the apparent trend for modeled gradients to be more intense than analyzed ones.

The results clearly indicate the tilting term to be the largest by far of the three moist adiabatic terms above the surface. As shown by OP, it is strongly negative (frontolytical) at a position along and slightly to the left of the vorticity maximum line. Figure 7b shows this to be the case because  $w_x$  is maximum here (while  $\theta_x > 0$ ). Since tilting dominates the other two adiabatic terms in this region, the frontogenetical function as the sum of these three terms alone in OP is quite negative, implying that strong frontolytical processes dominate here.

Previous model simulations (Orlanski and Ross, 1984) indicate that in moist convection the vertical advection of potential temperature (adiabatic cooling) is roughly compensated by latent heat release due to condensation. From that result, one would expect that in the presence of moist convection the tilting term (being derived from the horizontal gradient of this vertical advection) would be largely compensated by the corresponding diabatic term in (5.1). In other words, if the tilting term produces a frontolytical effect, the diabatic term will produce an opposing frontogenetical effect. The diabatic term, as calculated from the model solution (Fig. 9a), shows a similar structure to that of the tilting term in Fig. 8. As expected, large frontogenetical effects occur ahead of the vorticity maximum line. The sum of the tilting and diabatic terms is shown in Fig. 9b. Strong frontolytical effects occur on the cold side of the front, while weak frontogenesis is evident in the middle levels on the warm side ahead of the front. Diffusion (Fig. 9c) produces frontolysis which reinforces that shown in Fig. 9b on the cold side of the front.

Finally, with these additional terms now available, we are able to address the question of what terms contribute to frontogenesis and frontolysis. The substantial derivative of  $|\nabla_H \theta|$ , shown in Fig. 9d, is the true frontogenetical function.\* A strong frontolytical region exists on the

\* This term is computed independent of the other terms. The sum of all terms produces a residue of only  $16 \times 10^{-10} \text{ K m}^{-1} \text{ s}^{-1}$ .

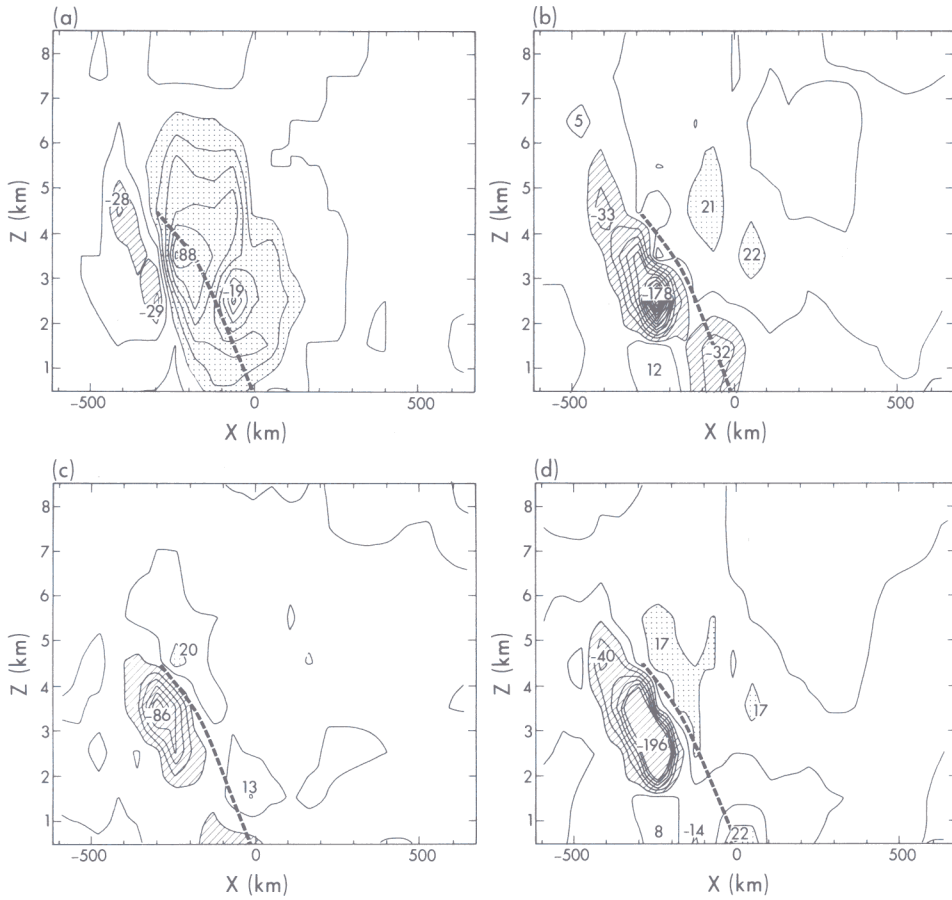


FIG. 9. Comparison of nonadiabatic terms and substantial derivative term in units of  $10^{-10} \text{ K m}^{-1} \text{ s}^{-1}$  with contour interval of  $12 \times 10^{-10} \text{ K m}^{-1} \text{ s}^{-1}$ . Cross-hatching and stippling indicate terms less than  $-12 \times 10^{-10} \text{ K m}^{-1} \text{ s}^{-1}$  and more than  $12 \times 10^{-10} \text{ K m}^{-1} \text{ s}^{-1}$ , respectively. (a) Diabatic, (b) diffusion, (c) diabatic and tilting, and (d) substantial derivative.

cold side of the front at middle levels, with tilting and diffusion being the largest contributors to the frontolysis. Regarding the intensity of this frontolytical effect, however, one should recognize that its large magnitude is due, in part, to the fact that  $|\nabla_H \theta|$  is generally small in this region (Fig. 7d). Two regions of frontogenesis appear on the warm side of the vorticity line, one near the surface and the other at around 5 km. The mechanisms for surface frontogenesis are convergence and deformation. The frontogenesis that occurs above 2 km seems to be largely due to the excess of the diabatic term over the tilting term (Fig. 9b).

These results are consistent with the differences evident between the moist and dry solutions above the low levels. They also seem to be consistent with our intuition that a moist frontal solution will have a deeper structure than a dry one. The accepted view has been that this deep circulation is associated with the moist convection ahead of the front and that the frontal circulation itself is not significantly altered by convection. In fact, the simulation indicates that the *entire* frontal circulation changes in a moist environment. In a dry environment, the main circulation of the front follows isentropic surfaces, whereas in a moist (saturated) environment, parcels follow moist pseudoadiabats (i.e., surfaces of constant equivalent potential temperature), thereby modifying the entire cross-stream circulation. The steeper slope of the frontal structure in the moist case is the result of the weaker static stability of the moist environment.

The present discussion can be extended to attempt to answer the question posed by Charney, mentioned at the beginning of this paper, as to how surface frontal waves are connected to upper-level baroclinic waves. We know how finite-amplitude waves produce frontogenesis and that the resulting surface fronts can be unstable (Eliassen, 1960; Orlanski, 1968). Now we can envision that, in a moist atmosphere, after surface frontal waves have developed due to secondary instabilities, they are able to communicate with the upper levels of the troposphere through the moist diabatic processes. This communication is achieved through the mechanism whereby short unstable frontal waves modulate areas of moist convection, thereby modifying the moist environment in the upper levels. We have shown above that the frontal circulation is not only modified directly by convective systems, but also feels the influence of the less stable moist environment.

The current level of our understanding of fronts provides us with considerable confidence in our understanding of the mechanisms governing the generation and maintenance of atmospheric fronts. On the other hand, there is a whole range of unanswered questions regarding secondary effects of fronts: How do fronts interact with orography and how are they associated with lee cyclogenesis? What conditions determine the type of moist convection, such as the many different kinds of rainbands, that fronts produce? How do fronts affect mesoscale convection in general? What role do fronts play in the generation of mesoscale convective complexes, comma clouds, and coastal cyclogenesis? A review of the progress made in these areas in recent years is beyond the scope of the present discussion. There is, however, considerable evidence that many mesoscale convective systems develop in association with a preexisting frontal system (Orlanski and Polinsky,

1984). While we have developed a good understanding of the main dynamics of frontal systems, there remain many opportunities for future advancement in these new areas. We have so far only scratched the surface in our understanding of how this important phenomenon, the front, interacts with other atmospheric systems.

#### ACKNOWLEDGMENTS

The authors, who were the members of the Mesoscale Group at the GFDL during the late period of Joseph Smagorinsky's tenure as director of the GFDL, would like to express our deep appreciation to him for his constant encouragement, support, and interest in mesoscale research. Also, regarding this chapter, the authors thank Professor William Blumen for his helpful review, Professor Yoshio Ogura for providing the photograph for Fig. 5, and Professor Frederick Sanders, Dr. Isaac Held, and Dr. Daniel Keyser for providing useful comments. Also, we appreciate the fine work done by Mrs. Joan Pege, Messrs. John Conner, Philip Tunison, Jeffrey Varanyak, and Michael Zadworne during the preparation of this paper.

#### REFERENCES

- Anthes, R. A., Kuo, Y.-H., Benjamin, S. G., and Li, Y.-F. (1982). The evolution of the mesoscale environment of severe local storms: Preliminary model results. *Mon. Weather Rev.* **110**, 1187–1213.
- Baines, P. G. (1980). The dynamics of the Southerly Buster. *Aust. Meteorol. Mag.* **28**, 175–199.
- Bjerknes, J. (1919). On the structure of moving cyclones. *Geophys. Norv.* **1**, No. 2.
- Bjerknes, J. (1937). Theorie der aussertropischen Zyklonenbildung. *Meteorol. Z.* **54**, 462–466.
- Bjerknes, J., and Solberg, H. (1921). Meteorological conditions for the formation of rain. *Geophys. Norv.* **2**, No. 3, 1–61.
- Blumen, W. (1980). A comparison between the Hoskins–Bretherton model of frontogenesis and the analysis of an intense surface frontal zone. *J. Atmos. Sci.* **37**, 64–77.
- Blumen, W. (1981). The geostrophic coordinate transformation. *J. Atmos. Sci.* **38**, 1100–1105.
- Boyd, J. P. (1980). The nonlinear equatorial Kelvin wave. *J. Phys. Oceanogr.* **10**, 1–11.
- Charney, J. (1947). The dynamics of long waves in a baroclinic westerly current. *J. Meteorol.* **4**, 35–162.
- Charney, J. (1975). Jacob Bjerknes—An Appreciation, in “Selected Papers of Jacob Aall Bonnevie Bjerknes” (M. G. Wurtele, ed.), pp. 11–13. Western Periodicals Company, North Hollywood, California.
- Decker, M. T. (1984). Observation of low-level frontal passages with microwave radiometers. In “Analysis of Some Cloud and Frontal Events, Recorded during the Boulder Upslope Cloud Observation (BOUCE) of 1982.” (E. E. Gossard, ed.), pp. 27–32. March 1984, NTIS #PB84-179662.
- Eady, E. (1949). Long waves and cyclonic waves. *Tellus* **1**, No. 3, 33–52.

- Eliassen, E. (1960). On the initial development of frontal waves. *Publ. Dan. Meteorol. Inst.* No. 13.
- Eliassen, A. (1959). On the formation of fronts in the atmosphere. In "The Atmosphere and the Sea in Motion" (B. Bolin, ed.), pp. 277–287. Rockefeller Inst. Press, New York.
- Eliassen, A. (1962). On the vertical circulation in frontal zones. *Geophys. Norv.* **24**, 147–160.
- Hoskins, B. J. (1982). The mathematical theory of frontogenesis. *Annu. Rev. Fluid Mech.* **14**, 131–151.
- Hoskins, B. J., and Bretherton, F. P. (1972). Atmospheric frontogenesis models: Mathematical formulation and solution. *J. Atmos. Sci.* **29**, 11–37.
- Hoskins, B. J., and Heckley, W. A. (1981). Cold and warm fronts in baroclinic waves. *Q. J. R. Meteorol. Soc.* **107**, 79–90.
- Hoskins, B. J., and West, N. V. (1979). Baroclinic waves and frontogenesis. Part II. Uniform potential vorticity jet flows—cold and warm fronts. *J. Atmos. Sci.* **36**, 1663–1680.
- Houghton, D. D. (1969). Effect of rotation on the formation of hydraulic jumps. *JGR, J. Geophys. Res.* **74**, 1351–1360.
- Keyser, D., and Anthes, R. A. (1982). The influence of planetary boundary layer physics on frontal structure in the Hoskins–Bretherton horizontal shear model. *J. Atmos. Sci.* **39**, 1783–1802.
- Kotschin, N. (1932). Über die Stabilität von Margulesschen Diskontinuitätsflächen. *Beitr. Phys. Atmos.* **18**, 129–164.
- Margules, M. (1906). Über Temperaturschichtung in stationar bewegter und ruhender luft. *Hann-Band. Meteorol. Z.*, pp. 243–254.
- Miller, J. E. (1948). On the concept of frontogenesis. *J. Meteorol.* **5**, 169–171.
- Ogura, Y., and Portis, D. (1982). Structure of the cold front observed in SESAME-AVE III and its comparison with the Hoskins–Bretherton frontogenesis model. *J. Atmos. Sci.* **39**, 2773–2792.
- Orlanski, I. (1968). Instability of frontal waves. *J. Atmos. Sci.* **25**, 178–200.
- Orlanski, I., and Polinsky, L. J. (1983). Ocean response to mesoscale atmospheric forcing. *Tellus* **35A**, 296–323.
- Orlanski, I., and Polinsky, L. J. (1984). Predictability of mesoscale phenomena. *Proc. Int. Symp. Nowcasting, 2nd, 1984. Norrköping, Sweden*, pp. 271–280.
- Orlanski, I., and Ross, B. B. (1977). The circulation associated with a cold front. Part I. Dry case. *J. Atmos. Sci.* **34**, 1619–1633.
- Orlanski, I., and Ross, B. B. (1984). The evolution of a cold front. Part II. Mesoscale dynamics. *J. Atmos. Sci.* **41**, 1669–1703.
- Palmen, E., and Newton, C. W. (1969). "Atmospheric Circulation Systems: Their Structure and Physical Interpretation (Int. Geophys. Ser., Vol. 13), Academic Press, New York.
- Pedlosky, J. (1979). "Geophysical Fluid Dynamics." Springer, New York.
- Pettersen, S. (1956). "Weather Analysis and Forecasting," 2nd ed., Vol. I. McGraw-Hill, New York.
- Phillips, N. A. (1956). The general circulation of the atmosphere: A numerical experiment. *Q. J. R. Meteorol. Soc.* **82**, 123–164.
- Rao, G. V. (1966). On the influence of fields of motion, baroclinicity, and latent heat source on frontogenesis. *J. Appl. Meteorol.* **5**, 377–387.
- Ross, B. B., and Orlanski, I. (1978). The circulation associated with the cold front. Part II. Moist Case. *J. Atmos. Sci.* **35**, 445–465.
- Ross, B. B., and Orlanski, I. (1982). The evolution of a cold front. Part I. Numerical simulation. *J. Atmos. Sci.* **39**, 296–327.

- Sanders, F. (1955). An investigation of the structure and dynamics of an intense surface frontal zone. *J. Meteorol.* **12**, 542-552.
- Sawyer, J. S. (1952). Dynamical aspects of some simple frontal models. *Q. J. R. Meteorol. Soc.* **78**, 170-178.
- Sawyer, J. S. (1956). The vertical circulation at meteorological fronts and its relation to frontogenesis. *Proc. R. Soc. London, Ser. A* **234**, 346-362.
- Solberg, H. (1928). Integrationen des atmosphärischen Störungsgleichungen. *Geophys. Norv.* **5**, No. 9.
- Williams, R. T. (1967). Atmospheric frontogenesis: A numerical experiment. *J. Atmos. Sci.* **24**, 627-641.
- Williams, R. T. (1974). Numerical simulation of steady-state fronts. *J. Atmos. Sci.* **31**, 1286-1296.
- Witham, G. B. (1974). "Linear and Non Linear Waves." Wiley, New York.